Journal of Power Sources 199 (2012) 170–173

Contents lists available at SciVerse ScienceDirect

Journal of Power Sources

journal homepage: www.elsevier.com/locate/jpowsour

Short communication

One-step sintering process of gadolinia-doped ceria interlayer–scandia-stabilized zirconia electrolyte for anode supported microtubular solid oxide fuel cells

Toshio Suzuki*, Bo Liang, Toshiaki Yamaguchi, Hirofumi Sumi, Koichi Hamamoto, Yoshinobu Fujishiro

National Institute of Advanced Industrial Science and Technology (AIST), Nagoya, Japan

ARTICLE INFO

Article history:
Received 10 August 2011
Received in revised form
23 September 2011
Accepted 13 October 2011
Available online 19 October 2011

Keywords:
SOFC
Electrolyte
Co-sintering
GDC
ScSZ
Fuel cell

ABSTRACT

A microtubular solid oxide fuel cell (SOFC) consisting of Gd-doped CeO_2 (GDC) interlayer–Sc stabilized zirconia (ScSZ) electrolyte has been prepared on an anode supported tube using one step sintering process at 1350 °C. The cell performance under high fuel utilization condition, with H_2 flow rate as low as 4.3 mL min^{-1} per 1 cm^2 electrode area is evaluated. The one-step sintering process results in an improvement of open circuit voltage but an increase of ohmic resistance due to possible high resistive layer and voids observed between GDC and ScSZ layers. The performance of the cell shows power densities of 0.35–0.57 W cm^{-2} with corresponding energy efficiencies of 45–20% (LHV), respectively, at 700 °C. Impedance analyses at different voltages have shown that the overpotential due to gas transport is dominant in the low current density region.

1. Introduction

Solid-oxide fuel cells (SOFCs), which are known to be high efficiency energy devices, have been intensively studied for a variety of applications [1–3]. In order to accelerate the commercialization of SOFCs, lowering the operating temperature of SOFCs is of importance, since it can broaden the selection of materials, and increase the life-time of the cell. So far, many studies related to lowering operating temperatures of SOFCs have been reported, mainly focusing on new electrode and electrolyte materials [4–9]. In addition, many research groups have put considerable efforts toward practical application, for examples, direct use of hydrocarbon fuels by selecting appropriate anode materials [10,11] and giving the stability to the cells under quick-startup/shutdown operation [12–14].

Developing a cost-effective fabrication process is another important issue for commercialization of SOFCs. In our previous study, we have shown that the conventional ceramic processes (extrusion and wet-slurry coating) can be applied to fabricate high performance microtubular type SOFC, using conventional, commercially available raw ceramic materials [15]. The fabrication process includes three successive stages of sintering, to make an electrolyte–anode support at 1350 °C, an interlayer (Gd-doped CeO_2 (GDC)) at 1200 °C, and a cathode at 1100 °C. The GDC interlayer acts as a protective layer to prevent a reaction between a cathode (especially, cobaltite perovskite type oxide) and a stabilized zirconia electrolyte to form $La_2Zr_2O_7$ and $SrZrO_3$ [16]. A shortcoming of the use of GDC is that it may react with the zirconia electrolyte to form $(Ce–Zr)O_2$ solid solutions at the interface at high sintering temperature above 1300 °C, which have high resistance. Thus, the sintering temperature of the interlayer must be carefully controlled. On the other hand, various different fabrication processes have been evaluated, and successful examples are the use of pulsed laser deposition (PLD) and co-sintering for fabricating dense Sm doped ceria layer on a zirconia electrolyte [17,18].

In this study, to seek for low cost fabrication process, a one step sintering process has been applied to the GDC interlayer–ScSZ electrolyte on the anode supported microtube and evaluated for cell performance. The cell was tested at high fuel utilization, where the cell performance was typically reduced. We then considered the effect of the co-sintering procedure on the energy efficiency of the single cell as a step toward module fabrication. Impedance analysis at different cell voltages was investigated in order to understand the contribution of electrochemical and gas transport processes on the cell performance in open circuit region.

2. Experimental

Cell fabrication process includes following four steps: (1) preparation of a clay mixture for anode tube extrusion and of slurries of an anode functional layer, an electrolyte, an interlayer, and a cathode

* Corresponding author. Tel.: +81 52 736 7083; fax: +81 52 736 7405.
E-mail address: toshio.suzuki@aist.go.jp (T. Suzuki).

0378-7753/$ – see front matter © 2011 Elsevier B.V. All rights reserved.
doi:10.1016/j.jpowsour.2011.10.046

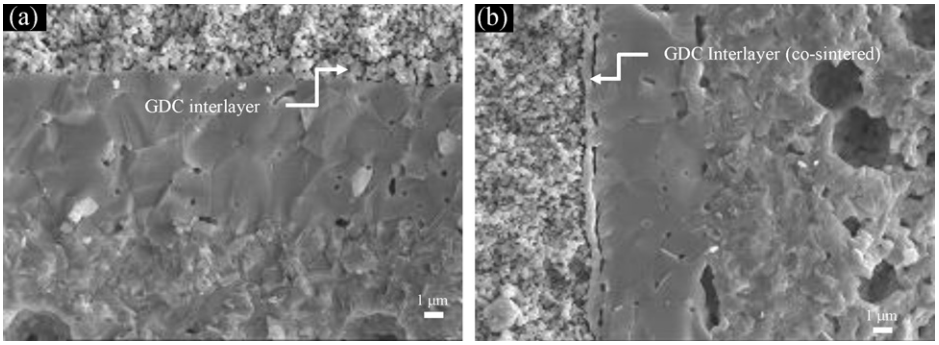

Fig. 1. The cross-sectional fracture SEM image of the microtubular SOFCs prepared using (a) conventional method and (b) one-step sintering process.

for coating process; (2) extrusion of the anode support tubes; (3) the coating process for the anode functional layer, the electrolyte, the interlayer and the cathode; and (4) the sintering process after each coating. The detailed fabrication process and materials for the standard cell were described elsewhere [19].

The microtubular SOFC consisted of an anode (60 wt%: NiO–40 wt%: 8 mol% yttria-stabilized zirconia (YSZ) as a tubular support), an anode functional layer (60 wt%: NiO–40 wt%: 10 mol% scandia-stabilized zirconia (ScSZ)), an electrolyte (ScSZ), an interlayer (10 mol% gadolinia-doped ceria (GDC)), and a cathode (70 wt%: $La_{0.6}Sr_{0.4}Co_{0.2}Fe_{0.8}O_{3-y}$ (LSCF)–30 wt%: GDC).

A one-step sintering process was applied to the ScSZ electrolyte–GDC interlayer. After extruding the anode tube from the clay mixture, the anode tubes were first dipped in the anode functional layer (NiO–ScSZ) slurry and dried in air. Second, they were dipped in the electrolyte (ScSZ) slurry and dried in air. Third, the tube coated with the anode functional layer and electrolyte were dipped in the interlayer (GDC) slurry, and co-sintered at 1350 °C for 1 h in air. Usually, the GDC interlayer coating is applied after the anode tube with the anode functional layer and the electrolyte has been co-sintered at 1350 °C for 1 h in air. The GDC interlayer is then sintered at 1200 °C. Finally, the cathode slurry was dip-coated and sintered at 1100 °C. The dimension of the resulting cell was 1.93 mm in diameter and 3 cm in length with the cathode length of 10 mm, and an effective electrode area of 0.61 cm^2. Note that this fabrication process is effective for controlling of the microstructure of the anode tube for the improvement of cell performance [20–22].

A scanning electron microscopy (SEM) (JSM6330F, JEOL Ltd, Tokyo, Japan) was utilized for the observation of the cell structure. The performance of the cell was studied using a potentiostat and impedance analyzer (Solartron Analytical, Hampshire, United Kingdom). Ag wire was used for collecting current from the electrodes, which were both fixed using Ag paste. The current collection from the anode side was made from an edge of the anode tube, and the collection from the cathode side was made from the whole cathode area. 20% H_2–Ar balance fuel was allowed to flow inside the anode tube at a flow rate of 13–47 mL min^{-1} (H_2 flow rate: 4.3–15.4 mL min^{-1} per 1 cm^2 electrode area) for power output performance testing. Air was supplied at the cathode side at a flow rate of 100 mL min^{-1}.

3. Results and discussion

Fig. 1 shows SEM images of the microtubular SOFCs prepared using (a) the conventional process (GDC interlayer separately sintered at 1200 °C); and (b) the one-step sintering process. As can be seen, while the GDC interlayer prepared using conventional method included large amount of pores among GDC grains (Fig. 1(a)), the co-sintered GDC interlayer became dense, although it included voids between the GDC interlayer and the electrolyte (Fig. 1(b)). This has also been observed in the literature [16,23], yet the mechanism of generating voids are not well understood. It is reported that unknown Zr–Sc–Ce–Gd oxide solid solution, which has low ionic conductivity, was detected at the interface and this is probably related to the formation of voids. Thus, an increasing in contact resistance is expected for cells prepared using one-step sintering process.

Fig. 2 shows the performance of the microtubular SOFCs prepared by the one-step sintering process at 700 °C furnace temperature at the fuel (20% H_2 in Ar) flow rate of 13–47 mL min^{-1}. The cell temperature at this furnace temperature was about 692 °C, and stable at each fuel flow rate. As can be seen, the performance of the cell showed 0.35, 0.42, 0.5, 0.55 and 0.57 W cm^{-2} maximum power density at fuel flow rates of 13, 17, 25, 34 and 47 mL min^{-1}, respectively. In our previous study [19], a cell prepared using the conventional process showed 0.52–0.88 W cm^{-2} at fuel flow rates of 17–47 mL min^{-1}, showing about 19% and 35% reduction from the maximum power density was observed at fuel flow rates of 17 and 47 mL min^{-1}, respectively. It is worth noting that the performance of the cell prepared using one-step sintering process reached a limiting value at high fuel gas flow rates, where the cell would be expected to show increased output power. The high resistance layer between the GDC interlayer and the electrolyte seemed to be the reason for this behavior. The advantage of the cell fabricated using one-step sintering process is seen to be the improvement in the open circuit voltage (OCV) to 1.08 V at the fuel flow rate of 17 mL min^{-1}, compared to 1.01 V for the conventional cell at the same condition. The dense GDC layer (reducing fuel crossover) is expected to improve fuel efficiency. Another possibility was

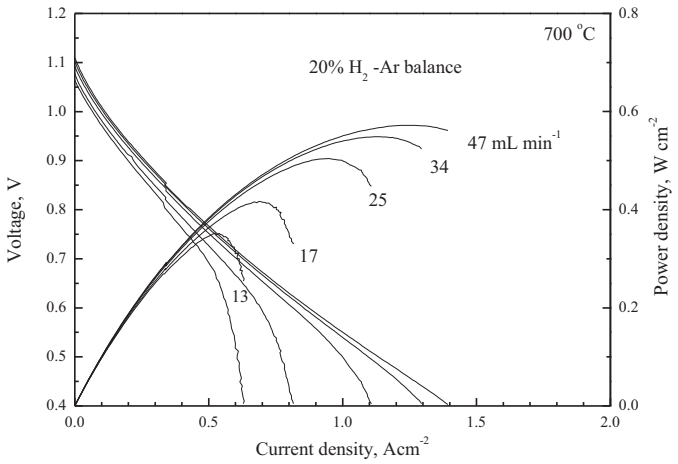

Fig. 2. The *IV* characterization of the cell prepared using the one-step sintering process at fuel (20% H_2 in Ar) flow rates of 13–47 mL min^{-1} at 700 °C.

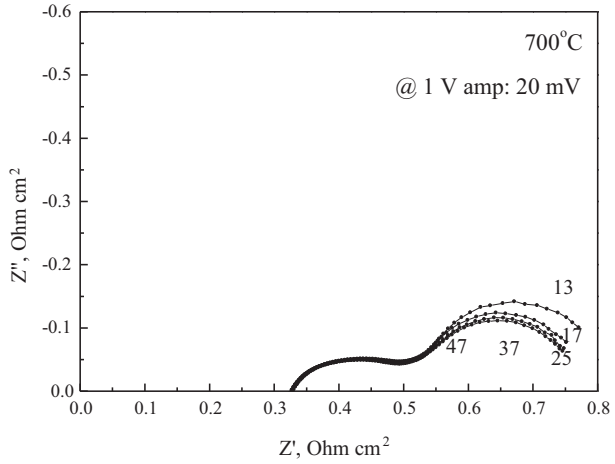

Fig. 3. Impedance spectra of the cell obtained at fuel (20% H_2 in Ar) flow rates of 13–47 mL min^{-1} at 700 °C.

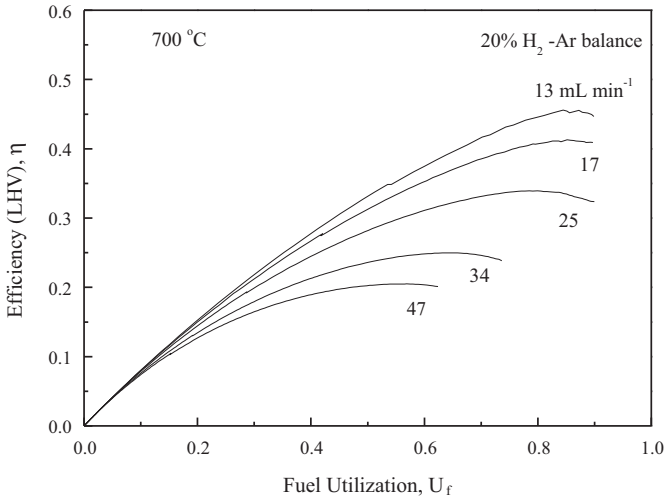

Fig. 4. The energy efficiency as a function of fuel utilization for the cell prepared using one step sintering process at 700 °C furnace temperature at various fuel flow rates.

that the GDC layer accelerated the densification of the electrolyte layer by diffusing Ce into the electrolyte. ScSZ does actually include 1 mol% of Ce for structural stabilization, and additional Ce may help stabilizing the cubic phase of zirconia.

Fig. 3 shows the impedance spectra at 700 °C furnace temperature obtained at 1.0 V with an amplitude of 10 mV for a cell prepared using one step sintering. Interpretations of the spectra may be found in the literature [24–26]. The lower frequency semi-circle became smaller as the fuel flow rate increased as previously reported, however, the degree of the change were relatively small compared to the conventional sample at 700 °C. At 700 °C, the area specific resistance of the electrolyte (5 μm thick ScSZ) is expected to be 0.015 Ω cm^2 [27], far below the value of the ohmic resistance, which corresponds to high frequency intercept shown in Fig. 3. Thus, we may account for the anode tube resistances because of its unique method of anode current collection [28], as well as the GDC interlayer and the cathode resistance. The observed ohmic resistance was 0.32 Ω cm^2, which was about 0.1 Ω cm^2 higher than that of a cell prepared using the conventional process [15] due to co-sintering of the GDC and ScSZ layers. In addition, not only the ohmic resistance but also the polarization resistances were increased for the cell prepared using the one-step sintering process. Thus, the effective contact area (electrode area) was reduced due to the presence of voids between the GDC layer and the electrolyte.

The lower heating value (LHV) energy efficiency was calculated by the equation, energy efficiency, $\eta = U_f \times V_{operation}/1.25$, where U_f and $V_{operation}$ are fuel utilization and the operating voltage, respectively. 1.25 V is the theoretical voltage for the following reaction [29],

$$H_2 + \tfrac{1}{2}O_2 \rightarrow H_2O \quad \text{(steam)} \qquad (1)$$

Since the fuel utilization is calculated using the operating current density and the fuel flow rate, the maximum energy efficiency can be given by the maximum power density per fuel flow rate. Fig. 4 shows the energy efficiency of the cell as a function of fuel utilization at 700 °C furnace temperature. The resulting energy efficiency of the cell increased from 20% to 45% when the fuel flow rate was decreased at 700 °C. Table 1 summarizes the relationship between the maximum energy efficiency and the maximum power density of the cell obtained at various fuel flow rates at 700 °C. High peak power densities of the cell were obtained at higher fuel flow rate by sacrificing energy efficiency, and as a result, power densities of 0.57 (efficiency: 20%) and 0.35 (efficiency: 45%) W cm^{-2} were obtained at 700 °C. This effect should carefully be considered in the further development toward SOFC systems.

Table 1
The relationship between the maximum energy efficiency and the maximum power density of the cell obtained at various fuel flow rates at 700 °C.

H_2 fuel flow rate (mL min^{-1} cm^{-2})	4.3	5.6	8.2	12.1	15.4
Max. P (W cm^{-2})	0.35	0.42	0.5	0.55	0.57
Efficiency (%)	45	41	34	25	20

Impedance analyses at different voltages were conducted at a fuel flow rate of 17 mL min^{-1} and the results are shown in Fig. 5. Fig. 5(a) shows the voltages for impedance measurements and the corresponding impedance spectra are shown in Fig. 5(b). The lower current density region is typically termed activation polarization, where it is considered that polarization for electrochemical reactions is dominant. The results, however, showed that overpotential due to gas transport (low frequency semi-circle) was dominant in the region close to the open circuit voltage and reduced as the current density was increased. Fig. 5(c), the magnified graph of Fig. 5(b), showed that the high frequency semi-circle is also reduced at higher current density, thus, the activation polarization was also decreased. Further investigation is necessary to understand this behavior, however, the results clearly indicated that gas transport phenomena could be a dominant factor for the fuel cell performance at lower current density region depending upon testing conditions, i.e., gas flow rate, and cell geometry.

In summary, the results obtained for a cell prepared using a one-step sintering process for GDC–ScSZ were comparable to those in the literature and may be effective for developing a low-cost SOFC fabrication process. Further improvement can be achieved by, for example, reducing the co-sintering temperature [30].

4. Summary

A microtubular solid oxide fuel cell (SOFC) consisting of Gd-doped CeO_2 (GDC) interlayer–Sc-stabilized zirconia (ScSZ) electrolyte was prepared on an anode supported tube using a one-step sintering process at 1350 °C and evaluated for cell performance at various fuel flow rates at 700 °C. The one-step sintering process results in an improvement of open circuit voltage but an increase of ohmic resistance due to possible presence of a high resistive layer and of voids observed between the GDC and ScSZ layers. The performance of the cell shows power densities of 0.35–0.57 W cm^{-2} at corresponding LHV energy efficiencies of 45–20% respectively,

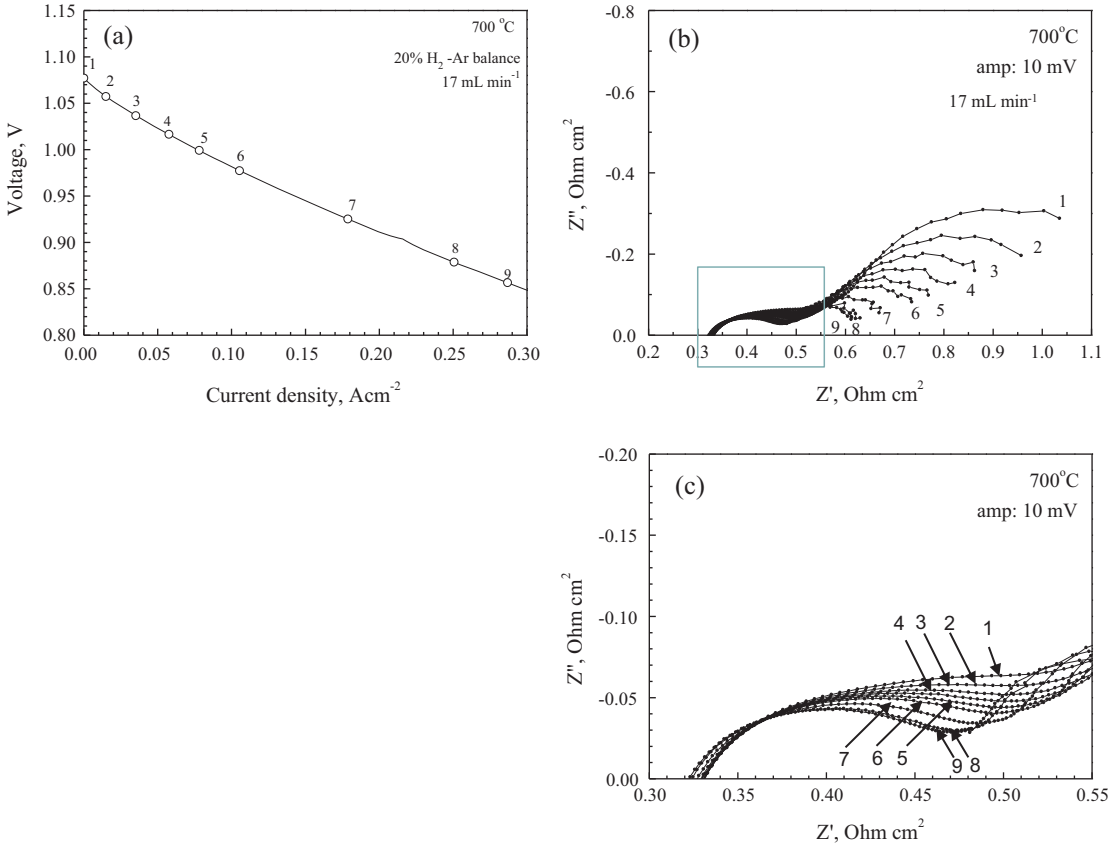

Fig. 5. (a) The *IV* characterization of the cell at the fuel flow rate of 17 mL min^{-1} at 700 °C in the low current density region (b) impedance spectra of the cell at different voltages obtained at the fuel flow rate of 17 mL min^{-1} at 700 °C and (c) a magnified graph of (b).

at 700 °C. Impedance analyses at different voltages have shown that the overpotential due to gas transport is dominant in the low current density region.

References

[1] N.Q. Minh, J. Am. Ceram. Soc. 78 (1993) 563–588.
[2] O. Yamamoto, Electrochim. Acta 45 (2000) 2423–2435.
[3] S.C. Singhal, Solid State Ionics 152–153 (2002) 405–410.
[4] H. Yokokawa, N. Sakai, T. Horita, K. Yamaji, M.E. Brito, MRS Bull. 30 (2005) 591–595.
[5] J.W. Yan, H. Matsumoto, M. Enoki, T. Ishihara, Electrochem. Solid-Sate Lett. 8 (2005) A389–A391.
[6] Z.P. Shao, S.M. Haile, Nature 431 (2004) 170–173.
[7] S.W. Tao, J.T.S. Irvine, Nat. Mater. 2 (2003) 320–323.
[8] K. Eguchi, T. Setoguchi, T. Inoue, H. Arai, Solid State Ionics 52 (1992) 165–172.
[9] T. Hibino, A. Hashimoto, K. Asano, M. Yano, M. Suzuki, M. Sano, Electrochem. Solid-Sate Lett. 5 (2002) A242–A244.
[10] R.J. Gorte, H. Kim, J.M. Vohs, J. Power Sources 106 (2002) 10–15.
[11] E.P. Murray, T. Tsai, S.A. Barnett, Nature 400 (1999) 649–651.
[12] N.M. Sammes, Y. Du, R. Bove, J. Power Sources 145 (2005) 428–434.
[13] K. Kendall, M. Palin, J. Power Sources 71 (1998) 268–270.
[14] K. Yashiro, N. Yamada, T. Kawada, J. Hong, A. Kaimai, Y. Nigara, J. Mizusaki, Electrochemistry 70 (2002) 958–960.
[15] T. Suzuki, S. Sugihara, K. Hamamoto, T. Yamaguchi, Y. Fujishiro, J. Power Sources 196 (2011) 5485–5489.
[16] T.L. Nguyen, K. Kobayashi, T. Honda, Y. Iimura, K. Kato, A. Neghisi, K. Nozaki, F. Tappero, K. Sasaki, H. Shirahama, K. Ota, M. Dokiya, T. Kato, Solid State Ionics 174 (2004) 163–174.
[17] D. Yang, X. Zhang, S. Nikumb, C. Decès-Petit, R. Hui, R. Maric, D. Ghosh, J. Power Sources 164 (2007) 182–188.
[18] X. Zhang, M. Robertson, C. Decès-Petit, Y. Xie, R. Hui, W. Qu, O. Kesler, R. Maric, D. Ghosh, J. Power Sources 175 (2008) 800–805.
[19] T. Suzuki, S. Sugihara, T. Yamaguchi, H. Sumi, K. Hamamoto, Y. Fujishiro, Electrochem. Commun. 13 (2011) 959–962.
[20] T. Suzuki, M.H. Zahir, Y. Funahashi, T. Yamaguchi, Y. Fujishiro, M. Awano, Science 325 (2009) 852–855.
[21] A.V. Virkar, J. Chen, C.W. Tanner, J.W. Kim, Solid State Ionics 131 (2000) 189–198.
[22] A. Bieberle, L.P. Meier, L.J. Gauckler, J. Electrochem. Soc. 148 (2001) A646–A656.
[23] T. Yamaguchi, S. Shimizu, T. Suzuki, Y. Fujishiro, M. Awano, J. Electrochem. Soc. 155 (2008) B423–B426.
[24] S.B. Adler, Solid State Ionics 111 (1998) 125.
[25] F. Zhao, A.V. Virkar, J. Power Sources 141 (2005) 79–95.
[26] S. Primdahl, M. Mogensen, J. Electrochem. Soc. 146 (1999) 2827–2833.
[27] Y. Mizutani, M. Tamura, M. Kawai, Solid State Ionics 72 (1994) 271–275.
[28] T. Suzuki, T. Yamaguchi, Y. Fujishiro, M. Awano, J. Power Sources 163 (2007) 737–742.
[29] J. Larminie, A. Dicks, Fuel Cell Systems Explained, Wiley, 2003.
[30] T. Suzuki, T. Yamaguchi, K. Hamamoto, H. Sumi, Y. Fujishiro, RSC Adv. 1 (2011) 911–916.